Bifurcation Micromechanics in Granular Materials

A. Wautier, J. Liu, François Nicot, F. Darve

Complete Book Title

Firstnamea LASTNAMEA
Firstnameb LASTNAMEB

April 5, 2016

Contents

Chapter 1

Bifurcation micromechanics in granular materials

1.1. Introduction

Plasticity, as induced by continuous irreversible rate-independent strains, is present in many engineering and natural materials. In this large framework, granular materials play a specific role due to the non-associate character of their plastic strains (the normality rule of the plastic incremental strain vectors to the elastic/yield surface is not fulfilled). This non-associativeness is essentially due to a Mohr-Coulomb plastic limit condition which gives rise to conical shapes for both the elastic/yield surface and the plastic limit surface. An associated flow rule with conical surfaces would then result in plastic increments $\mathbf{d}\boldsymbol{\varepsilon}^p$ with large volumetric part $\mathrm{Tr}\mathbf{d}\boldsymbol{\varepsilon}^p$ which is very far from the experimental observations for all geomaterials (soils, rocks and concrete). This is certainly the most important difference between conventional metal plasticity and granular plasticity.

Now, the elasto-plastic theory shows that non-associate plasticity imposes that the tangent constitutive tensor does not respect the so-called "major symmetry". Thus the elasto-plastic matrix is no more symmetric. As the bifurcations are linked to the singularities of this matrix, it becomes clear that the classes of bifurcations which can be expected from this non-symmetric matrix are a lot more diverse than in associate (symmetric) plasticity. Indeed, in associate plasticity, the bifurcations correspond to the singularities of the constitutive elasto-plastic matrix, thus (most often) to the vanishing of the determinant of this matrix on the plastic limit surface. On the other hand,

---

Chapter written by Antoine WAUTIER and Jiaying LIU and François NICOT and Félix DARVE.

in non-associate plasticity, bifurcations and failures can occur largely before reaching the Mohr-Coulomb plastic limit, like for example in the case of an undrained triaxial loading applied on a loose sand [DAO 09]. Also, the failure modes can be different. For example, we observe in labs and in situ that, for geomaterials, the failure can be localized with shear, compaction or dilation bands or it can also occur and develop without any visible macro-patterning like, for example, in the famous "sand liquefaction" phenomenon. This kind of quasi-homogeneous failure has been called "diffuse failure" [KHO 06].

If we limit our analyses to divergence instabilities (letting apart flutter instabilities and, more generally, geometric instabilities), it appears that the general criterion [LER 13] to study these bifurcations is the so-called "second order work criterion" as introduced by [HIL 58] and applied to geomaterials since several decades [DAR 87]. An overview about the applications of this criterion in geomechanics with experimental, theoretical and numerical approaches can be found in [WAN 16]. The link between this criterion and failure is recalled in the next section of this chapter by showing that, when the second order work takes negative values and some proper loading variables are applied, a burst of kinetic energy appears leading to a transition from a quasi-static deformation regime to a dynamic one [NIC 12b], which is typical of a failure development. We find here the basic reason why the second order work criterion can predict the accurate conditions for an effective failure.

The second order work criterion corresponds to the loss of positive definitiveness of the elasto-plastic matrix. So, according to linear algebra, when the determinant of the symmetric part of this matrix is negative, there is a cone of directions where the second order work takes negative values. This cone has been called "instability cone" [DAR 00] and its existence and shape will be shown through a Discrete Element Method (DEM) applied to a numerical cubical sample of spheres in section 1.2. In associate plasticity, the material bifurcations appear on the plastic limit condition. Since, in non-associate plasticity, the bifurcations are linked to the loss of positive definitiveness of this matrix (or equivalently of its symmetric part), the large differences between observed failures in metal plasticity and in granular plasticity finds here its basic explanation. Until now, the expression of the second order work has been considered in the framework of continuous mechanics. It takes the following form in small strains and by neglecting geometrical effects:

$$W_2 = \mathbf{d}\boldsymbol{\sigma} : \mathbf{d}\boldsymbol{\varepsilon}, \tag{1.1}$$

However granular materials are discrete by nature and it is necessary to consider a discrete expression related to intergranular forces and displacements. It can be conjectured that the unstable contacts are characterized by negative values of their discrete second order works computed for those contacts. The purpose of section 1.3 is to evaluate this point. So, the spatial distribution of the grain contacts with negative values of their second order works (called c^- contacts) is investigated in case of localized failure by shear band formation.

Besides it has been observed experimentally and numerically by DEM simulations that two classes of meso-structures play a central role in the strength/deformation behavior of granular materials: these are the so-called "force chains" and "grain loops" [SIB 15]. Roughly speaking the force chains are mainly responsible for the strength of the material, while the grain loops are responsible for its deformational characteristics. The complex interplay between these meso-structures is analysed in sub-sections 1.3.3 and 1.3.4. Basically the grain loops support laterally the force chains. While load is applied, force chains bend and then buckle at failure. Letting aside the micro-scale at grain level by considering now this meso-scale, it is interesting to understand and analyze the failure mechanisms at this intermediate scale.

Eventually section 1.4 is devoted to compare both the major regimes of failure evoked previously: the localized one and the diffuse one, all being described by the second order work criterion as divergence instabilities. The localized failure appears when, in addition to the second order work criterion, the localization criterion by shear band formation is fulfilled [RIC 76]. Let us note that, to respect consistency, the localization criterion can be verified only when the second order work criterion is itself fulfilled [NIC 11]. So, in this section 4, in spite of these different criteria, it will be shown that the failure micro-structures have the same characteristics inside the localized bands (when the failure is localized) and in the whole sample (for a diffuse failure). Indeed failure of granular materials corresponds to an uniquely given assembly organization, independently of the failure mode (localized or diffuse).

1.2. Application of the second order work criterion at REV scale

As recalled in section 1.1, the mechanical stability can be effectively assessed thanks to the second order work criterion. The bifurcation domain is then defined as the set of states where there exists at least one incremental loading path leading to the vanishing of the second order work. If such an incremental loading exists, a suitable choice in the control parameters will result in a brutal transition from a quasi-static to an inertial regime characterized by a sharp increase in kinetic energy. This transition is a consequence of the writing of the energy balance. Indeed, for a given mechanical system originally in an equilibrium state, its variation in kinetic energy is a second order term d^2E_c which equals to the difference between the external second order work at the boundary and the volume integral of the second order work [NIC 07, NIC 09, NIC 12b]. Let Ω denote a mechanical system within the boundary $\partial\Omega$. Let $\delta\boldsymbol{f}$ be the force per surface unit applied on $\partial\Omega$ and $\delta\boldsymbol{u}$ be the corresponding displacement on $\partial\Omega$. Then the variation of kinetic energy from an equilibrium state to any new infinitely close state reads

$$\begin{aligned} \mathrm{d}^2E_c &= |\Omega| \left(\overline{W}_2^{\mathrm{ext}} - \overline{W}_2 \right) \\ &= \int_{\partial\Omega} \delta\boldsymbol{f} \cdot \delta\boldsymbol{u} \, \mathrm{d}S - \int_{\Omega} W_2 \, \mathrm{d}V \end{aligned} \tag{1.2}$$

where $\overline{W}_2^{\text{ext}} = \frac{1}{|\Omega|}\int_{\partial\Omega} \delta \boldsymbol{f} \cdot \delta \boldsymbol{u} \, \mathrm{d}S$ is referred to as the mean external second order work and $\overline{W}_2 = \frac{1}{|\Omega|}\int_{\Omega} W_2 \, \mathrm{d}V$ is the mean (internal) second order work. W_2 is the local second order work computed at the material point scale following equation 1.1 for small strains.

In practice forces and displacements can only be measured on the boundary of sample volume. Based on these boundary quantities, only the external second order work can be computed. As a result, this fundamental equation has strong implications with respect to stability assessment at the material point scale:

- The initial state must be an equilibrium state ($E_c = 0$ and $\mathrm{d}E_c = 0$)

- In the final state the kinetic energy must be equal to zero ($\mathrm{d}^2E_c = 0$) in order to identify $\overline{W}_2^{\text{ext}}$ with $\overline{W}_2$.

By keeping in mind these two remarks, a stress controlled systematic procedure to assess the mechanical stability of a granular material at the material point scale is formulated as follows:

(1) prepare a sample in an initial equilibrium state by waiting for the kinetic energy to be negligible under a given constant mechanical stress state;

(2) perform a directional analysis by imposing stress (or strain) probes in several directions (in order to identify $\overline{W}_2^{\text{ext}}$ with $\overline{W}_2$ it is important to wait for the kinetic energy to return to its initial level);

(3) assess the negativeness of the second order work by computing the external second order work associated to each stress (or strain) probe;

(4) determine whether the considered material is in its bifurcation domain for the mechanical state and the microstructure considered.

In this section, a 3D cubic sample of 10 000 particles is used for illustrative purpose. It is prepared in a loose state and in a mechanical state corresponding to a drained triaxial loading up to a stress ratio $\eta = \frac{q}{p} = 0.45$ where p corresponds to the mean pressure and q to the deviatoric stress. The lateral confining pressure is kept to 100 kPa during the mechanical test. Figure 1.1 shows the numerical sample used in DEM simulations as well as its mechanical response while subjected to a drained triaxial test. More details can be found in [WAU 18].

When the target stress ratio is reached, the external control is switched from strain to stress in the axial direction (σ_{zz}) and kept constant until an equilibrium state is reached. This pre-stabilization step is necessary because of the inherently dynamic formulation of DEM codes.

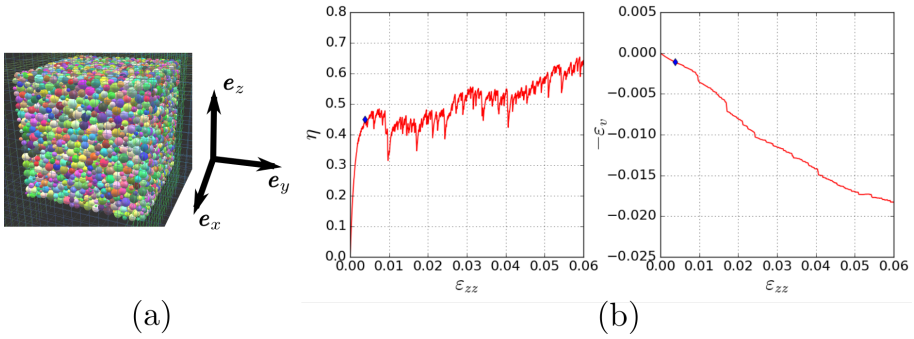

Figure 1.1. *Visualisation of the 3D sample used in this section (a) and drained triaxial response under a confining pressure of 100 kPa(b). The mechanical state $\eta = 0.45$ used in the present directional analysis is shown as a blue diamond point.*

From the reached equilibrium state, a stress directional analysis is performed in the plane of axisymmetry such that $\mathrm{d}\sigma_{xx} = \mathrm{d}\sigma_{yy}$ (Rendulic's plane). This procedure is commonly used and details can be found in [BAR 94, SIB 09, NIC 07, NIC 09, WAU 18]. In this plane $(\sqrt{2}\mathrm{d}\sigma_{xx}, \mathrm{d}\sigma_{zz})$, a stress increment $\mathbf{d\boldsymbol{\sigma}}$ is fully described by its polar coordinates $||\mathbf{d\boldsymbol{\sigma}}||$ and θ such that

$$\left\{ \begin{array}{rcl} \sqrt{2}\mathrm{d}\sigma_{xx} & = & ||\mathbf{d\boldsymbol{\sigma}}|| \cos\theta \\ \mathrm{d}\sigma_{zz} & = & ||\mathbf{d\boldsymbol{\sigma}}|| \sin\theta \\ ||\mathbf{d\boldsymbol{\sigma}}|| & = & \sqrt{\mathrm{d}\sigma_{zz}^2 + 2\,\mathrm{d}\sigma_{xx}^2} \end{array} \right. . \tag{1.3}$$

In practice, finite stress increments of 5 kPa are imposed in the form of a constant stress loading rate followed by a stabilization phase on the sample boundaries [WAU 18]. As both initial and final states are equilibrium states, Hill-Mandel lemma holds and an incremental stress tensor $\mathbf{d\boldsymbol{\sigma}}$ can be defined from boundary stresses. To each incremental loading $\mathbf{d\boldsymbol{\sigma}}$ corresponds a strain increment $\mathbf{d\boldsymbol{\varepsilon}}$. Based on these quantities a normalized second order work is then defined at the material point scale (REV scale) as

$$W_2^{\mathrm{norm}} = \frac{\mathbf{d\boldsymbol{\varepsilon}} : \mathbf{d\boldsymbol{\sigma}}}{||\mathbf{d\boldsymbol{\varepsilon}}||\,||\mathbf{d\boldsymbol{\sigma}}||} \tag{1.4}$$

The sign of this quantity is then sufficient to detect whether the considered incremental direction is stable ($W_2^{\mathrm{norm}} > 0$) or unstable ($W_2^{\mathrm{norm}} < 0$). The result of the directional analysis can be represented as a polar diagram with coordinates $(\theta, W_2^{\mathrm{norm}})$ or in a circular diagram in which an offset is used to avoid negative radii in the polar coordinates. As visible in Figure 1.2 the circular envelope corresponding to the tested

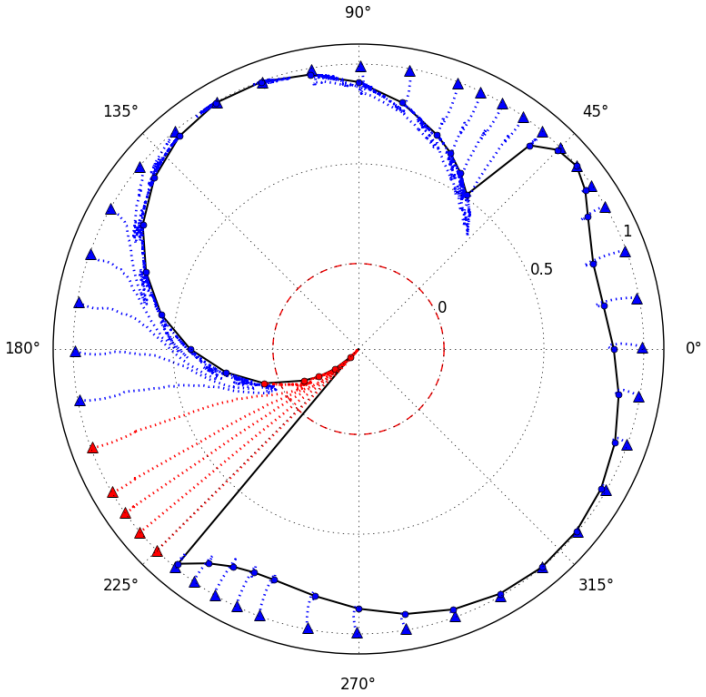

Figure 1.2. *Circular diagram of the normalized second order work for* $\eta = 0.45$ *and* $||\mathbf{d}\boldsymbol{\sigma}|| = 5$ kPa *(solid black). Transient evolution of* $\dfrac{W_2^{\mathrm{ext}}(t)}{||\mathbf{d}\boldsymbol{\varepsilon}(t)||\,||\mathbf{d}\boldsymbol{\sigma}(t)||}$ *are shown in dotted lines between the initial (triangle) and final states (circle) of the directional analysis. Directions with transient vanishing of* W_2^{ext} *are shown in red.*

sample exhibits a cone of instability for $\theta \in [205°, 225°]$ where $W_2^{\mathrm{norm}} < 0$. As a result the considered sample in its current state (mechanical and microstructure states) is inside the bifurcation domain.

Complementary to the classical circular envelope $(\theta, W_2^{\mathrm{norm}})$ plotted in Figure 1.2 [SIB 09, WAU 18], time evolutions of $W_2^{\mathrm{ext}}(t)$ can be computed based on reaction stresses and displacements on the sample boundary. Provided that the increase in kinetic energy is limited, an incremental stress tensor $\mathbf{d}\boldsymbol{\sigma}(t)$ can be defined at any time from boundary stresses as well as an effective loading angle $\theta(t)$ in Rendulic's plane. If no loss of controllability (in the sense of Nova [NOV 94]) is observed, this effective loading angle is constant as imposed by the incremental loading program. However, because of microstructure modifications, transient losses of controllability

might occur. In Figure 1.2, dotted lines correspond to circular representations of

$$\left(\theta(t), \frac{W_2^{\text{ext}}(t)}{||\mathbf{d}\boldsymbol{\varepsilon}(t)||\ ||\mathbf{d}\boldsymbol{\sigma}(t)||}\right)$$

In this figure, transient losses of controllability are observed for some directions in which the parametric curve $\left(\theta(t), \frac{W_2^{\text{ext}}(t)}{||\mathbf{d}\boldsymbol{\varepsilon}(t)||\ ||\mathbf{d}\boldsymbol{\sigma}(t)||}\right)$ does not follow straight lines. As the normalized external second order work decreases, the incremental stress loading direction $\theta(t)$ deviates toward the direction of the cone of instability. During this transient process, the parametric curve $\left(\theta(t), \frac{W_2^{\text{ext}}(t)}{||\mathbf{d}\boldsymbol{\varepsilon}(t)||\ ||\mathbf{d}\boldsymbol{\sigma}(t)||}\right)$ stays slightly outside the final normalized second order work envelope. As soon as the transient softening regime is stopped, $\mathbf{d}\boldsymbol{\sigma}(t)$ gets back to the targeted direction. This deviation is consistent with the energy balance giving $W_2^{\text{ext}} > W_2$. For some directions a transient vanishing of W_2^{ext} can even be obtained (see $\theta = 200^\circ$ for instance). For future developments, these transient evolutions should be considered systematically in the numerical assessment of instabilities thanks to the second order work criterion.

1.3. From macro to micro analysis of instability

In Section 1.2, the notion of instability is defined at the material point scale. Within the homogenization framework, the mechanical behavior of a given material at this scale can be recovered by considering a representative elementary volume. While zooming in this volume, it is possible to link the vanishing of the second order work to micromechanics.

1.3.1. *Local second order work and contact sliding*

Besides the second order work definition recalled in the introduction within a continuum mechanics framework, W_2 can be derived from microscopic variables describing the granular material microstructure while considering the interparticle reaction [NIC 07, NIC 12a, HAD 13, SIB 15]. Let $\boldsymbol{l}^c$ be the branch vector connecting the two centers of a contacting pair of particles in contact, $\boldsymbol{F}^c$ the inter-particulate contact force, $\boldsymbol{F}^p$ the resultant contact force on particle p and $\boldsymbol{x}^p$ the position of its mass center. Then W_2 reads at the material point scale

$$W_2 = \frac{1}{|\Omega|}\left(\sum \delta F_i^c \delta l_i^c + \sum \delta F_i^p \delta x_i^p\right) \tag{1.5}$$

where Ω is a representative elementary volume of granular material.

Provided that only quasi-static evolutions are considered, W_2 reduces to the first term and a microscopic form of second order work can be defined at the contact scale as $w_2^c = \delta F_i^c \delta l_i^c$ [NIC 06].

Thanks to this definition, two categories of contacts are defined according to the sign of w_2^c. In the following text c^- is used to designate contacts with strictly negative values of w_2^c [HAD 13, SIB 15] (compared with the cited references we exclude the condition $w_2^c = 0$ which may correspond to contacts with unchanged forces and relative displacements). The condition $w_2^c < 0$ is associated with local failure, i.e. contact sliding [NIC 06, NIC 13]. In this case Mohr-Coulomb criterion is fulfilled at the microscopic scale through a decrease in the normal contact force [NIC 13]. Besides, if an effective failure is triggered, local second order work w_2^c will be concentrated in a specific domain in which bursts of kinetic energy will occur simultaneously [NIC 12b, DAR 04].

Based on the previous comments a sliding potential I_p is introduced to describe the contact state as:

$$I_p = F_t/(F_n tan\varphi) \tag{1.6}$$

where F_n and F_t are the magnitudes of normal and tangential forces, and φ is the friction angle at the contact scale. I_p lies in $[0, 1]$ with $I_p = 1$ meaning that the sliding condition is absolutely fulfilled.

Considering the spatial distribution of c^- and sliding contacts when failure occurs, intuitive images of a 2D specimen suffering shear banding are shown in Figure 1.3 (More details in [LIU 17]). For the sake of comparison, incremental deviatoric strain distribution are plotted in Figure 1.3(a). It is clear that both the c^- contacts and contacts close to sliding ($I_p > 0.99$) are concentrated within the shear band area. Similar results of w_2^c were shown for different loading paths [SIB 15]. Therefore at the microscopic scale, the second order work criterion, contact sliding and instabilities are highly correlated.

1.3.2. *Role of strong contact network on stable and unstable loading directions*

As recalled in subsection 1.3.1, contact sliding is a necessary condition to result in a microscopic vanishing of the second order work, and c^- contacts play an important role in local failure characterization. For a granular material within the bifurcation domain, the role of strong contact network is significant [HAD 13]. Following [RAD 98] the overall contact system is splitted into two populations of contacts:

- strong contacts transmitting contact forces larger than the average
- weak contacts transmitting contact forces smaller than the average

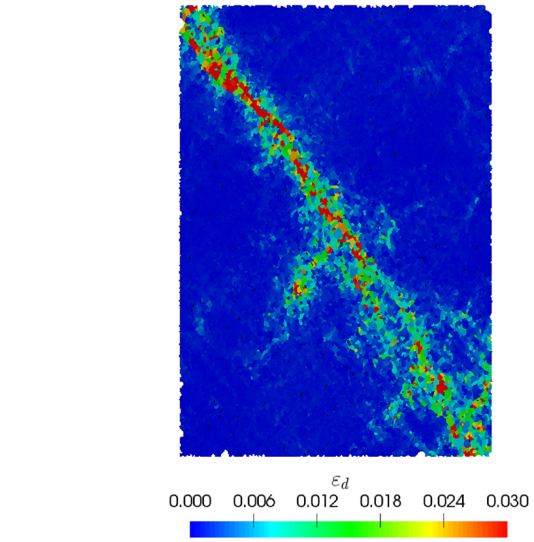

(a)

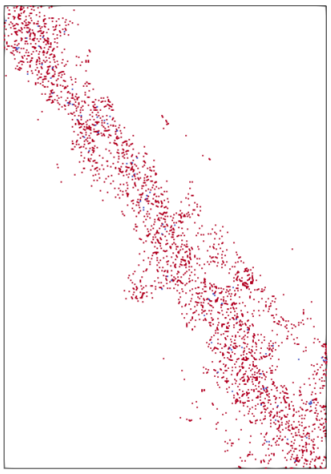

(b)

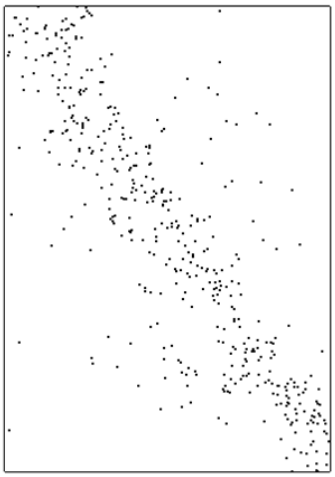

(c)

Figure 1.3. *Spatial distribution of contacts with negative microscopic second order work and contacts close to sliding: (a) incremental deviatoric strain distribution; (b) c^- contacts; (c) contacts close to sliding ($I_p > 0.99$).*

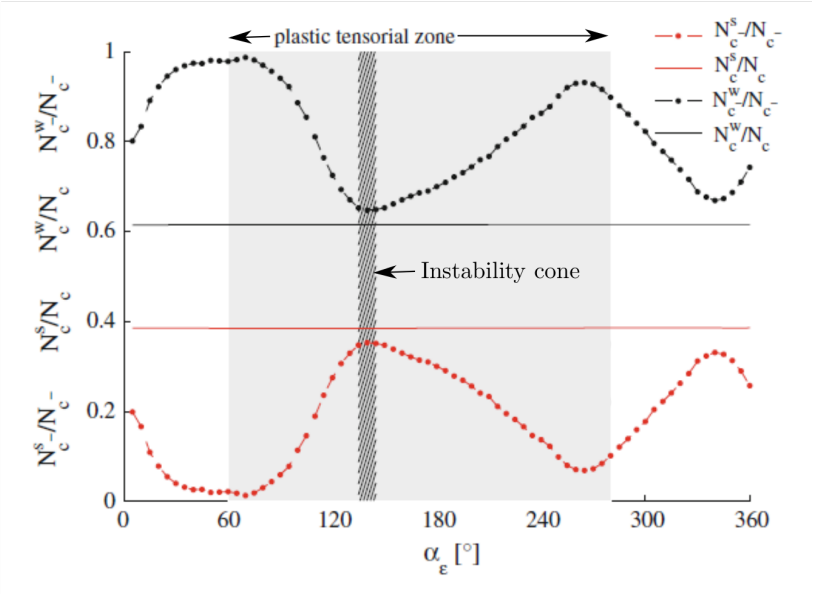

Figure 1.4. *Repartition of sliding contacts with $w_2^c < 0$ between strong and weak contact networks with respect to the incremental strain loading direction α_ε [HAD 13]*

In [HAD 13], the authors presented a strain controlled directional analysis carried out on a sample within the bifurcation domain. The overall contact network was composed of roughly 40 % of strong contacts (N_c^s/N_c) and 60 % of weak ones (N_w^s/N_c) for all loading directions. N_{c^-} denotes the number of contacts with negative second order work $w_2^c < 0$. Among this population of c^- contacts, it is then interesting to distinguish those belonging to strong ($N_{c^-}^s$) and weak ($N_{c^-}^w$) contact networks. In Figure 1.4, the fractions $N_{c^-}^s/N_{c^-}$ and $N_{c^-}^w/N_{c^-}$ are given for different strain loading directions α_ε, which shows different partitions in comparison with the overall contacts.

In this figure, the plastic tensorial zone is shown in light grey and the cone of instability in hatching. The cone of instability is characterized by a high proportion of strong c^- contacts while outside the cone in the plastic zone, c^- contacts are more likely to be found in the weak phase. This result highlights that a negative macroscopic second order work originates from microscopic modifications destabilizing the strong contact network that loses its bearing capacity.

1.3.3. *From contact sliding to mesoscale mechanisms*

As a great deal of the complex mechanical behavior of granular materials is due to geometrical effects, a contact scale description of granular materials is usually not

sufficient to explain the macroscopic behavior. Therefore a mesoscopic scale is often introduced to capture the elementary mechanisms. At the scale of a few grains, force chains and loops (in 2D), may be defined to account for the stress transmission as well as volumetric changes [ZHU 16b, TOR 10]. Force chains are always related to the strong contact network mentioned in Section 1.3.2, moreover, they are defined by incorporating more geometrical considerations [PET 05]. The bending of force chains and topological changes of 2D loops are regarded as loss of sustainability at meso-scale, which shows strong correlations with contact sliding [LIU 17].

Force chains mainly contribute to the elastic strength of the assembly, while contact sliding is an indication of plastic dissipation. It is well accepted that sliding contacts are excluded from the strong contact network [RAD 98], however, force chain bending often occurs close to contact sliding positions. According to the definition of force chains [PET 05], force chain bending is defined at the scale of 3-particle group inside force chains as a deviation from geometrical linearity [ZHA 17, ZHU 16b, TOR 07, WAU 18]. In order to correlate the bending and its surrounding contact sliding a mean particle sliding index S_{rp} can be computed as follows [LIU 17]:

(1) For each 2D meso-loop i, compute the proportion of sliding contacts as $S_{rl}^i = N_s^i/N_c^i$, where N_s^i is the number of sliding contacts within loop i and N_c^i the total number of contacts within loop i;

(2) Identify all loops containing a given particle p, name the loop set as L_p and average the sliding proportion S_{rl}^i for $i \in L_p$ to define a particle sliding index S_{rp}^p as

$$S_{rp}^p = \frac{1}{N_{lp}} \sum_{i \in L_p} S_{rl}^i, \tag{1.7}$$

where N_{lp} is the cardinal of L_p;

(3) For a given group of particles, the associated mean sliding index S_{rp} is defined by averaging particle's sliding indices S_{rp}^p. By definition $S_{rp} \in [0, 1]$ and a large S_{rp} value corresponds to a large fraction of sliding contacts in the loops surrounding the considered group of particles.

Considering a biaxial test for a dense frictional granular assembly [LIU 17], the evolutions of S_{rp} along axial strain are shown in Figure 1.5 for different particle groups. It is clear that S_{rp} computed for all bending groups of three chained particles exhibits higher values than those for the two other groups of particles considered. This result supports the fact that force chain bending is linked to surrounding contact sliding. According to previous studies [ZHU 16b, TOR 07], force chain bending firstly appears at the point near the characteristic point (the most compressive state of deviatoric loading, before stress peak) and reaches a high magnitude at the stress peak. In fact, before the characteristic point, elastic mechanisms dominate and only few sliding contacts exist, homogeneously distributed within the assembly. After this point, sliding

develops around force chains, which result in force chain bending. This explains the reason why a transition is observed before stress peak in Figure 1.5.

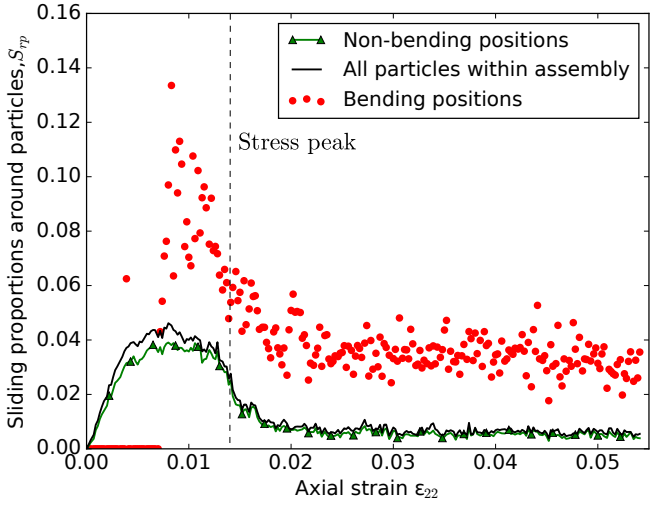

Figure 1.5. *Evolution of sliding proportions around particles S_{rp}, for three groups: bending particles within force chains; non-bending particles within force chains; all particles in the assembly.*

For 2D granular materials, the kinematic constraints existing between grains can be characterized through topological changes in the loop structures. From an incremental point of view, existing loops can topologically

- keep constant: a loop of N grains stays incrementally unchanged (called "Future_NC" hereafter)

- get smaller: a loop of N grains disappears between two incremental states and its grains form smaller loops (called "Future_NS" hereafter)

- get larger: a loop of N grains incorporates new grains between two incremental states (called "Future_NL" hereafter)

Figure 1.6 illustrates the evolution of average sliding proportions S_{rl} of 3 kinds of 6-grain loops (Future_6C, Future_6S and Future_6L) versus axial strain during a drained biaxial loading. Data of Figure 1.6 is from the same biaxial simulation as Figure 1.5. As Future_6L demonstrates a higher value of sliding proportion, we can conclude that contact sliding mainly induces loop enlargement.

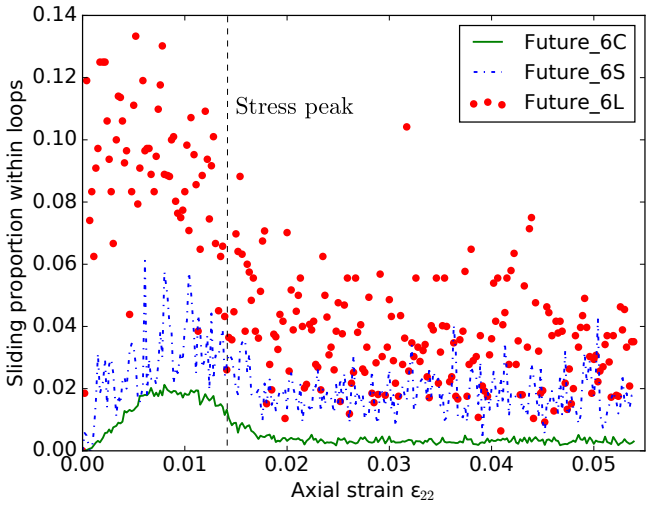

Figure 1.6. *Evolution of sliding proportions of 6-grain loops owning 3 kinds of futures: keep constant, Future_6C; become smaller, Future_6S; become lager, Future_6L.*

1.3.4. *Micromechanisms leading to bifurcation at the REV scale*

In [ZHU 16b, TOR 10], the authors concluded that at the mesoscale, there is an interplay between force chains and grain loops. As sliding mostly occurs within loops in contact with force chains, the decreasing of kinematic constraints around force chains may enable force chain to bend and collapse more easily.

To look into the process of the kinematic constraints decrease and the failure scenario at the REV scale, the numerical procedure presented in Section 1.2 is used, focusing on an unstable loading direction $\theta = 210.5°$. The release in kinematic constraints around force chains is directly linked to the decrease in the number of contacts between chained and non-chained particles. By dividing the contacts into three groups, namely chained/chained (cc), non-chained/non-chained (nn) and non-chained/chained (nc) contacts, the time evolutions of the sizes of the three populations can be tracked during an incremental loading leading to the vanishing of second order work ($\theta = 210.5°$). These evolutions are shown in Figure 1.7. During the incremental loading, the microstructure reorganization is linked to the onset and propagation of a burst of kinetic energy which is indicated in Figure 1.7 by two vertical solid lines (more details may be found in [WAU 18]).

In Figure 1.7 the onset of the kinetic burst is strongly linked to an early decrease in N_{nc} which results in a deconfinement of force chains. Complementary to this

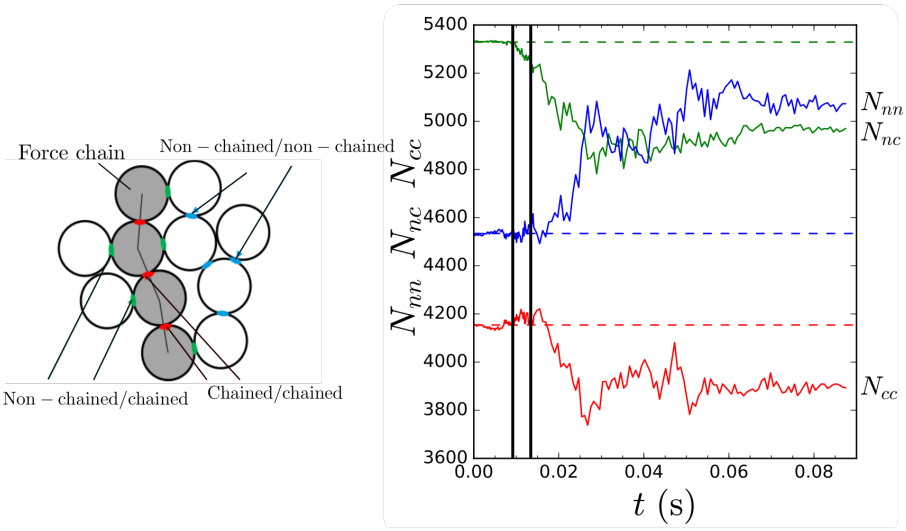

Figure 1.7. *Time evolution of N_{nn}, N_{nc} and N_{cc} during an incremental loading leading to the vanishing of the second order work ($\theta = 210.5^\circ$). The onset of the mechanical instability is associated with a kinetic burst of energy indicated by two vertical solid lines.*

observation, one can look at the time evolution of the loss of controllability: the mean bending rate of groups of three chained particles ($\dot{\beta}$, where β is the deviation angle from the straight line, and $\dot{}$ stands for its time derivative) and the mean kinetic energy per particle. These evolutions are shown in Figure 1.8 for the whole sample and for a control volume defined around the location where the burst of kinetic energy initiates.

These graphs confirm that the release in kinematic constraints around force chains will result in bending mechanisms which is visible at the REV scale as a loss of controllability. As force chain bending does not stop, existing force chains eventually disappear and the microstructure reorganizes as a whole which results in plastic strain development at the REV scale.

1.4. Diffuse and localized failure in a unified framework

As recalled in the introduction the second order work W_2 is a material point scale quantity which requires the definition of a REV. When shear band appears during the deviatoric loading, the specimen is no more homogeneous and cannot be regarded as a material point. In this section we would like to show how similar are the micromechanics in homogeneous samples suffering from different patterns of failure.

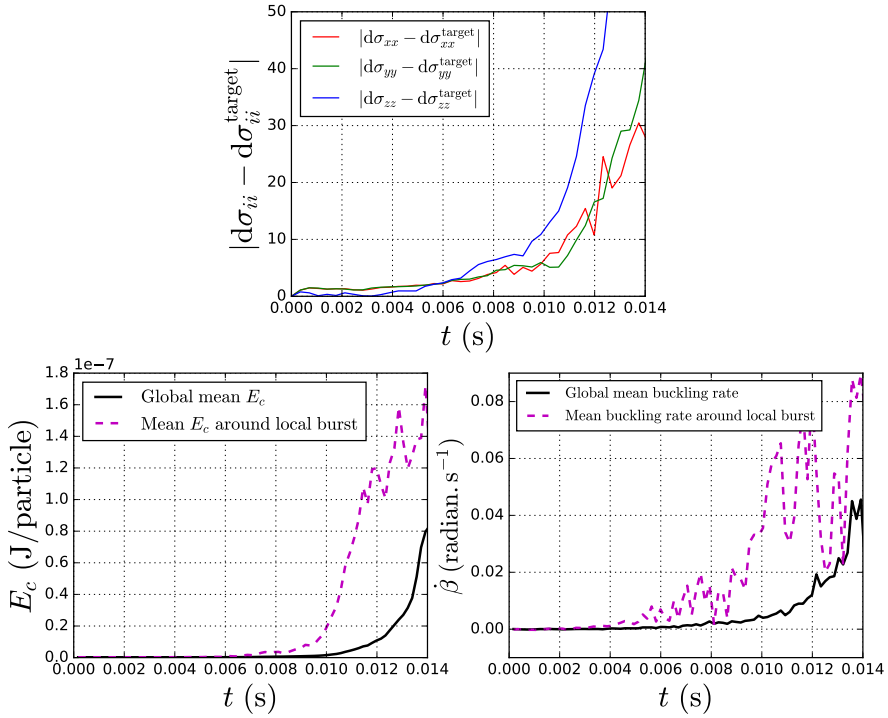

Figure 1.8. *Time evolution of the difference between measured incremental stresses and their setpoint value (top), mean kinetic energy per particle (left) and mean bending rate of groups of three chained particles (right) [WAU 18]. The considered sample is the one introduced in section 1.2 for a mechanical state $\eta = 0.45$ and an incremental stress loading direction $\theta = 210.5°$. Dashed lines represent averaged quantities in a control volume located close to the onset of the kinetic burst indicating microstructure reorganizations.*

1.4.1. *Diffuse and localized failure pattern*

Granular materials in their bifurcation domain can indeed fail following two different kind of failure patterns, namely diffuse or localized [ZHU 16a, SIB 15]. If the localized failure is at stake, homogeneity of the considered sample is lost and the problem of interest has to be treated as a boundary value problem. Consequently the notions of REV and bifurcation point vanish.

Figure 1.9 shows the comparison between two microstructures undergoing a drained biaxial test. One corresponds to a dense state with a well marked localized failure in the form of a shear band, and one corresponds to a loose state for which a diffuse failure is observed. Following the results presented in the previous section, failure is triggered by force chain bending. As mentioned in Section 1.3.4, for each group of

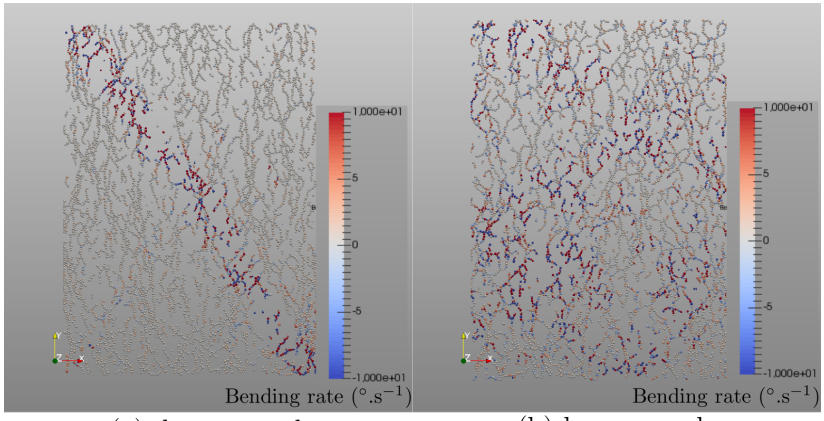

(a) dense sample (b) loose sample

Figure 1.9. *Failure patterns for a dense (a) and a loose (b) sample during a drained biaxial test. Only chained particles are shown and colored according to the local bending rates of elementary groups of three chained particles.*

three particles, if β denotes the deviation angle from the straight line, a bending rate can be defined with respect to the axial strain ε as $\frac{\mathrm{d}\beta}{\mathrm{d}\varepsilon}$.

For the dense sample, large bending rates $\frac{\mathrm{d}\beta}{\mathrm{d}\varepsilon}$ concentrate in a diagonal persistent zone whereas in the loose one, large bending rates form evanescent clusters distributed in all the specimen. Another important observation is that large positive bending rates (associated with deviations from the straight line configuration) and large negative bending rates (corresponding to evolutions closer to the straight line configuration) tends to concentrate at the same spots. A possible explanation for that might come from force chains forming (replacing the buckled ones) due to microstructural reorganizations.

1.4.2. *Common micromechanisms and microstructures*

As shown in [ZHU 16a], localized and diffuse failure modes have been proved to be identical within internal structures, i.e., the strain localized domain owns the same micromechanical characteristics as the diffuse failure case. The void ratio is regarded as one of the most important critical state parameters, Figure 1.10 gives the evolutions of void ratios for dense and loose specimens under biaxial drained loading [ZHU 16a]. Convergent values are observed for loose specimen and the localized domain of dense specimen (shear band area).

Besides the void ratio, the fabric anisotropy represents another important common aspect. Figure 1.11 exhibits the second deviatoric invariant of local fabric tensors

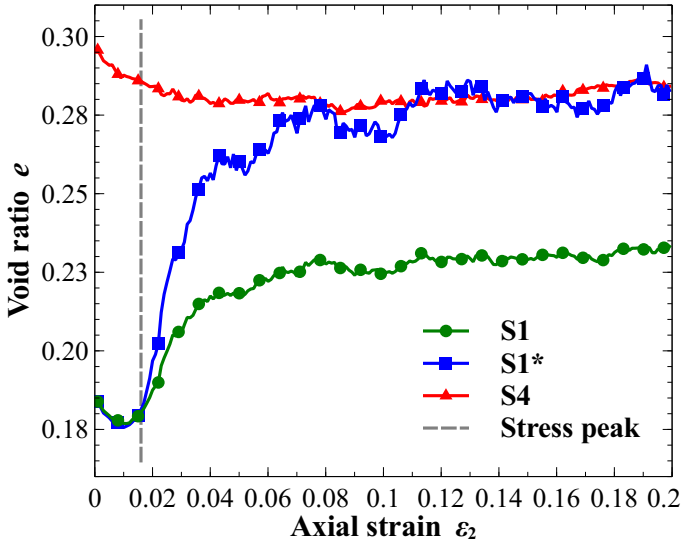

Figure 1.10. *Void ratios for dense and loose granular assemblies subjected to biaxial test [ZHU 16a]: S1 denotes dense assembly; S1* denotes shear band area of dense assembly; S4 denotes loose assembly.*

within loops [ZHU 16a], which further identifies a unique microstructure for localized and diffuse failure.

Following the definitions introduced in section 1.3.3 the strain evolution of S_{rp} around bending particles within force chains are shown in Figure 1.12 for both dense and loose granular assemblies undergoing drained biaxial test. For the dense case in which a shear band forms, S_{rp} is also computed particularly in the shear band area. After the failure point (or stress peak of the dense assembly), both the dense and loose specimens demonstrate the same micro scale mechanism with $S_{rp} \sim 0.035$. And no difference is identified between the whole dense assembly and the shear band area, because the contact sliding concentrates inside the shear band area. In addition to the microstructure geometry, Figure 1.12 highlights the fact that the failure micromechanisms are similar in the loose and dense assemblies.

1.5. Conclusion

This Chapter has pointed out the importance of the second-order work criterion to detect the existence of an unstable state. More specifically, for a given material volume and after a given loading history, the mechanical state of a granular material is reputed to be unstable by divergence if some loading directions leading to an outburst in kinetic

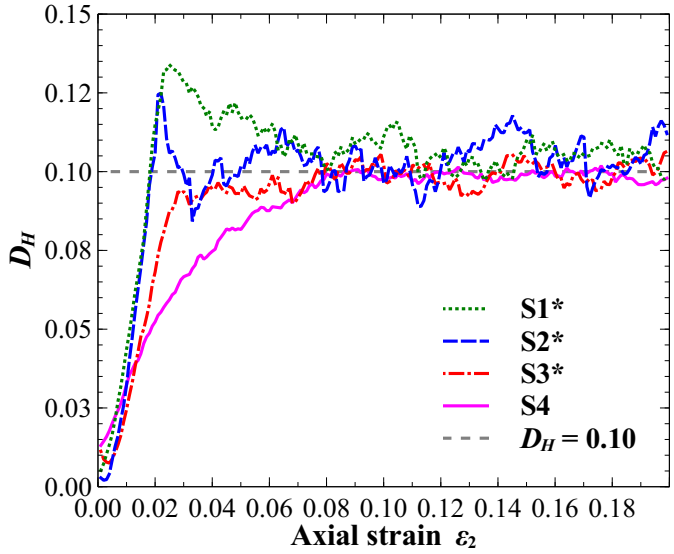

Figure 1.11. *Second deviatoric invariant of local fabric tensors [ZHU 16a]: S1*, S2* and S3* denote shear band area of dense or medium dense assemblies; S4 denotes loose assembly.*

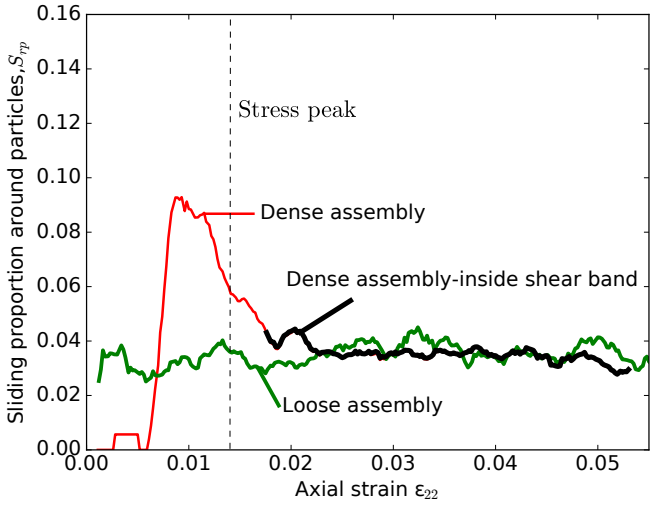

Figure 1.12. *Sliding proportions around bending particles for dense and loose assemblies during a drained biaxial test.*

energy exist. Such directions will be associated with negative values of the internal second-order work.

Interestingly, the internal second-order work cannot be computed readily even at the scale of a representative elementary volume (REV). As the accessible variables are those acting on the boundary of the specimen, the external second-order work is computed instead. Taking advantage of the fundamental equation stating that the second-order increase in kinetic energy equals to the difference between the external and internal second-order works, it appears that the external second-order work (recalling that the kinetic energy is always positive) constitutes an upper bound of the internal second-order work. In particular, if the external second-order work is negative, so is the internal second-order work.

Taking advantage of DEM-based numerical simulations run on two-dimensional specimens, local information is available on the contact scale between granules, making it possible to compute the second-order work from microscopic quantities. Thus, the vanishing of the microscopic second-order work can be related to some geometrical features of the local packing on the mesoscale. This micro to macro link has highlighted the major role played by two grain meso-structures: force chains and grain loops. These two kind of meso-structures in close interaction, strongly govern the mechanical strength and the deformational properties of the specimen. In particular, it is shown that grain rearrangements affecting loops in contact with force chains are prone to destabilize these force chains, contributing to the strength limit of the specimen. These rearrangements involve grain sliding, probably resulting from macroscopic dilatancy.

These conclusions, mostly based and motivated by strong physical arguments, will have to be confirmed in a three-dimensional context. If it can be thought that the physics pointed out so far should be preserved, it must be noted that a quantitative description will be much more challenging, as the local packings (force chains, grain loops) will be also much more difficult to describe from a topological point of view.

1.6. Bibliography

[BAR 94] BARDET J.-P., "Numerical simulations of the incremental responses of idealized granular materials", *International Journal of Plasticity*, vol. 10, num. 8, p. 879–908, Elsevier, 1994.

[DAO 09] DAOUADJI A., ALGALI H., DARVE F., ZEGHLOUL A., "Instability in granular materials: experimental evidence of diffuse mode of failure for loose sands", *Journal of Engineering Mechanics*, vol. 136, num. 5, p. 575–588, American Society of Civil Engineers, 2009.

[DAR 87] DARVE F., CHAU B., "Constitutive instabilities in incrementally non-linear modelling", *Constitutive laws for engineering materials*, p. 301–310, Elsevier: Amsterdam, 1987.

[DAR 00] DARVE F., LAOUAFA F., "Instabilities in granular materials and application to landslides", *Mechanics of Cohesive-frictional Materials*, vol. 5, num. 8, p. 627–652, Wiley Online Library, 2000.

[DAR 04] DARVE F., SERVANT G., LAOUAFA F., KHOA H., "Failure in geomaterials: continuous and discrete analyses", *Computer methods in applied mechanics and engineering*, vol. 193, num. 27, p. 3057–3085, Elsevier, 2004.

[HAD 13] HADDA N., NICOT F., BOURRIER F., SIBILLE L., RADJAI F., DARVE F., "Micromechanical analysis of second order work in granular media", *Granular matter*, vol. 15, num. 2, p. 221–235, Springer, 2013.

[HIL 58] HILL R., "A general theory of uniqueness and stability in elastic-plastic solids", *Journal of the Mechanics and Physics of Solids*, vol. 6, num. 3, p. 236–249, Elsevier, 1958.

[KHO 06] KHOA H. D. V., GEORGOPOULOS I. O., DARVE F., LAOUAFA F., "Diffuse failure in geomaterials: Experiments and modelling", *Computers and Geotechnics*, vol. 33, num. 1, p. 1–14, Elsevier, 2006.

[LER 13] LERBET J., KIRILLOV O., ALDOWAJI M., CHALLAMEL N., NICOT F., DARVE F., "Additional constraints may soften a non-conservative structural system: Buckling and vibration analysis", *International Journal of Solids and Structures*, vol. 50, num. 2, p. 363–370, Elsevier, 2013.

[LIU 17] LIU J., NICOT F., ZHOU W., Sustainability of internal structures during shear band forming in 2D granular materials, Submitted to journal, under review, 2017.

[NIC 06] NICOT F., DARVE F., "Micro-mechanical investigation of material instability in granular assemblies", *International Journal of Solids and Structures*, vol. 43, num. 11, p. 3569–3595, Elsevier, 2006.

[NIC 07] NICOT F., SIBILLE L., DONZE F., DARVE F., "From microscopic to macroscopic second-order work in granular assemblies", *Mechanics of Materials*, vol. 39, num. 7, p. 664–684, Elsevier, 2007.

[NIC 09] NICOT F., SIBILLE L., DARVE F., "Bifurcation in granular materials: An attempt for a unified framework", *International Journal of Solids and Structures*, vol. 46, num. 22, p. 3938–3947, Elsevier, 2009.

[NIC 11] NICOT F., DARVE F., "Diffuse and localized failure modes: two competing mechanisms", *International Journal for Numerical and Analytical Methods in Geomechanics*, vol. 35, num. 5, p. 586–601, Wiley Online Library, 2011.

[NIC 12a] NICOT F., HADDA N., BOURRIER F., SIBILLE L., WAN R., DARVE F., "Inertia effects as a possible missing link between micro and macro second-order work in granular media", *International Journal of Solids and Structures*, vol. 49, num. 10, p. 1252–1258, Elsevier, 2012.

[NIC 12b] NICOT F., SIBILLE L., DARVE F., "Failure in rate-independent granular materials as a bifurcation toward a dynamic regime", *International Journal of Plasticity*, vol. 29, p. 136–154, Elsevier, 2012.

[NIC 13] NICOT F., HADDA N., DARVE F., "Second-order work analysis for granular materials using a multiscale approach", *International Journal for Numerical and Analytical Methods in Geomechanics*, vol. 37, num. 17, p. 2987–3007, Wiley Online Library, 2013.

[NOV 94] NOVA R., "Controllability of the incremental response of soil specimens subjected to arbitrary loading programmes", *J. Mech. Behav. Mater*, vol. 5, num. 2, p. 193–201, 1994.

[PET 05] PETERS J., MUTHUSWAMY M., WIBOWO J., TORDESILLAS A., "Characterization of force chains in granular material", *Physical review E*, vol. 72, num. 4, Page041307, APS, 2005.

[RAD 98] RADJAI F., WOLF D. E., JEAN M., MOREAU J.-J., "Bimodal character of stress transmission in granular packings", *Physical review letters*, vol. 80, num. 1, Page 61, APS, 1998.

[RIC 76] RICE J. R., "The localization of plastic deformation", *IUTAM Congress on Theor. and Appl. Mech*, North-Holland Amsterdam, p. 207-220, 1976.

[SIB 09] SIBILLE L., NICOT F., DONZÉ F.-V., DARVE F., "Analysis of failure occurrence from direct simulations", *European Journal of Environmental and Civil Engineering*, vol. 13, num. 2, p. 187–201, Taylor & Francis, 2009.

[SIB 15] SIBILLE L., HADDA N., NICOT F., TORDESILLAS A., DARVE F., "Granular plasticity, a contribution from discrete mechanics", *Journal of the Mechanics and Physics of Solids*, vol. 75, p. 119–139, Elsevier, 2015.

[TOR 07] TORDESILLAS A., "Force chain buckling, unjamming transitions and shear banding in dense granular assemblies", *Philosophical Magazine*, vol. 87, num. 32, p. 4987–5016, Taylor & Francis, 2007.

[TOR 10] TORDESILLAS A., WALKER D. M., LIN Q., "Force cycles and force chains", *Physical Review E*, vol. 81, num. 1, Page011302, APS, 2010.

[WAN 16] WAN R., NICOT F., DARVE F., *Failure in Geomaterials, a contemporary treatise*, ISTE/Elsevier, 2016.

[WAU 18] WAUTIER A., BONELLI S., NICOT F., Micro-inertia origin of instabilities in granular materials, Accepted in International Journal for Numerical and Analytical Methods in Geomechanics, 2018.

[ZHA 17] ZHANG L., NGUYEN N. G. H., LAMBERT S., NICOT F., PRUNIER F., DJERAN-MAIGRE I., "The role of force chains in granular materials: from statics to dynamics", *European Journal of Environmental and Civil Engineering*, vol. 21, num. 7-8, p. 874–895, Taylor & Francis, 2017.

[ZHU 16a] ZHU H., NGUYEN H. N., NICOT F., DARVE F., "On a common critical state in localized and diffuse failure modes", *Journal of the Mechanics and Physics of Solids*, vol. 95, p. 112–131, Elsevier, 2016.

[ZHU 16b] ZHU H., NICOT F., DARVE F., "Meso-structure organization in two-dimensional granular materials along biaxial loading path", *International Journal of Solids and Structures*, vol. 96, p. 25–37, Elsevier, 2016.